High-Q resonant modes in a photonic crystal heterostructure nanocavity and applicability to a Raman silicon laser

Yasushi Takahashi,[1,2,*] Yoshitaka Inui,[3,†] Masahiro Chihara,[1,†] Takashi Asano,[3] Ryo Terawaki,[1] and Susumu Noda[3,4,‡]

[1]*Nanoscience and Nanotechnology Research Center, Research Organization for the 21st Century, Osaka Prefecture University, Sakai, Osaka, 599-8570, Japan*

[2]*Japan Science and Technology Agency, PRESTO, Kawaguchi, Saitama 332-0012, Japan*

[3]*Department of Electronic Science and Engineering, Kyoto University, Kyoto, 615-8510, Japan*

[4]*Photonics and Electronics Science and Engineering Center, Kyoto University, Kyoto 615-8510 Japan*

(Received 21 August 2013; revised manuscript received 2 December 2013; published 26 December 2013)

When a heterostructure is created at the center of a photonic crystal line-defect cavity to form a nanocavity, the photonic band gap contains several high-quality (Q) factor resonant modes. We have studied the optical properties of these modes to examine their applicability to Raman silicon lasers, which require two high-Q resonant modes with a frequency spacing of 15.6 THz. Our experimental and numerical analyses reveal four types of resonant modes. We demonstrate that pairing the resonant mode originating from the first-order propagation mode with that arising from the second-order propagation mode is the most promising approach toward the realization of Raman silicon lasers.

DOI: 10.1103/PhysRevB.88.235313 PACS number(s): 42.55.Ye, 42.55.Tv, 42.55.Sa, 42.70.Mp

I. INTRODUCTION

Because silicon (Si) has an indirect band gap, with radiative electron-hole recombination of very low efficiency, the realization of Si-based lasers has proved to be difficult.[1] Instead of utilizing the interband transition, stimulated Raman scattering (SRS) in Si rib waveguides has been proposed as a route to achieve optical gain.[2] The Raman gain coefficient of crystalline Si is as high as that of commonly used Raman laser materials.[3] Furthermore, Si rib waveguides fabricated on Si-on-insulator (SOI) substrates exhibit tight confinement of light that enhances the SRS.[4] Therefore, this method has succeeded in achieving net optical gain[5–13] and has resulted in the continuous-wave (cw) operation of Raman Si lasers.[14] However, these lasers need the assistance of reverse-biased p-i-n diodes in order to remove the free carriers generated by two-photon absorption[15] and they have thresholds as high as 20 mW, even when a high-quality (Q) ring-cavity structure on the cm scale is used.[16]

We have recently reported on the realization of a μm-scale Raman Si laser with an ultralow threshold of 1 μW, using a photonic crystal (PC) heterostructure nanocavity without any p-i-n diode.[17] A key aspect was the exploitation of an unusual pair of high-Q resonant modes to confine the pump light and Stokes Raman scattered light inside the cavity. We utilized the ground-state heterostructure nanocavity modes that originate from the first-order and second-order propagation modes associated with the line defect forming the cavity (Fig. 1). However, the optical properties of the nanocavity mode created by the second-order mode have not been studied in detail. Furthermore, many higher-order resonant modes with high Q factors can be formed in a heterostructure cavity. Therefore, all these resonant modes should be investigated and their suitability for Raman Si lasers should be analyzed in detail.

In this article, we report on the whole set of high-Q resonant modes that are formed within the photonic band gap (PBG) for a two-step heterostructure cavity. By examining various properties of these modes (Q value, frequency, electric field distribution, and modal symmetry), we show that the ground-state heterostructure nanocavity modes originating from the two propagation modes are the most suitable pair for utilization in Raman Si lasers.

II. SAMPLE STRUCTURE

Nanocavities in two-dimensional (2D) PC slabs are exceptional optical resonators possessing both high Q factors and small volumes.[18–25] Figure 1(a) shows the structure of the samples studied here. A 2D PC consisting of a triangular lattice of circular air holes with radii of 110 nm was formed in a 220-nm-thick Si slab. The fundamental lattice constant a_1 was 410 nm. The upper line defect formed by a missing row of air holes is the excitation waveguide used to inject light into the cavity. The lower line defect formed by 39 missing air holes is the cavity that gives rise to the resonant modes for the Raman laser. The width (w) of the excitation waveguide and the distance from the cavity (l) were varied in different samples, as explained later. The width of the cavity was $\sqrt{3}a_1 = 710$ nm (W1). Figure 1(b) presents the band diagram of the cavity in the x direction, which is divided into five frequency regions. These regions were identified from the photonic band structure [Fig. 1(c)] for the line defect forming the cavity, which was calculated by the three-dimensional (3D) finite-difference time domain (FDTD) method. The PBG corresponds to the range between the two slab modes. The line defect supports two propagation modes inside the PBG, whose dispersion relations are denoted by dashed and solid curves. We classify them as the odd-propagation mode and even-propagation mode, respectively, based on the symmetry of their electric fields E_y with respect to the xz plane of the line defect (see Fig. 4). Total internal reflection at the slab-air interface results in low-loss propagation for both modes below the light line (dotted line), and the corresponding frequency ranges for each mode are shaded the same color as their dispersion relation curves. The mode gap is the band that does not contain any propagation mode.

A two-step heterostructure nanocavity was created at the center of the structure as shown in Fig. 1(a). The lattice

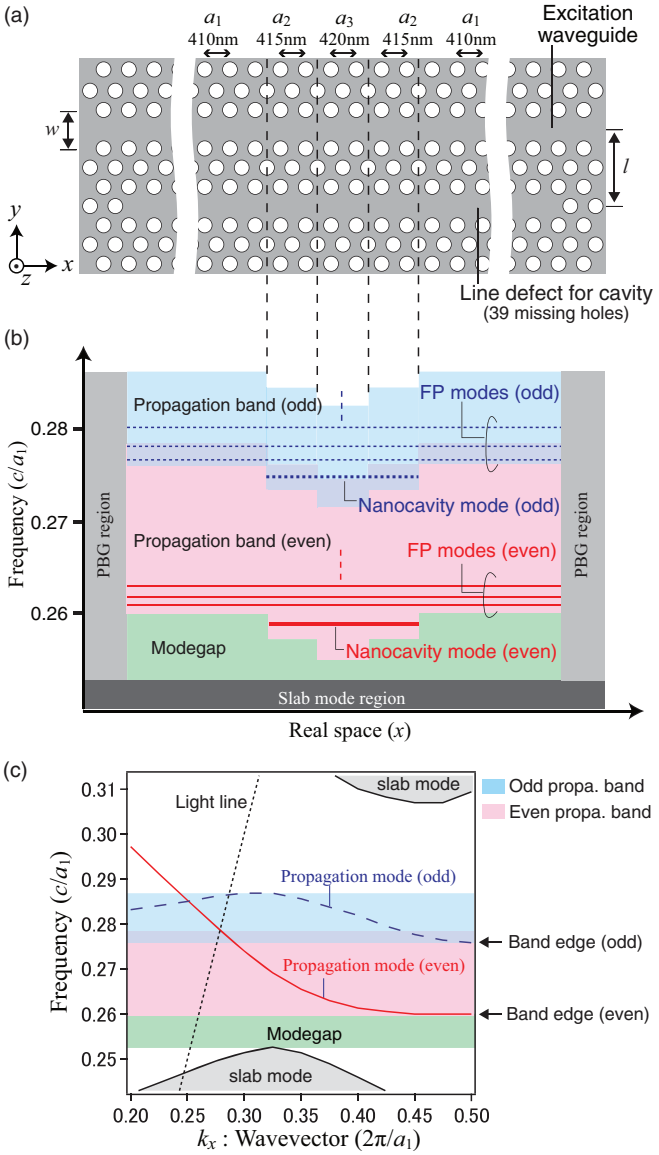

FIG. 1. (Color) (a) Schematic of a measured nanocavity sample. (b) Band diagram for the cavity in the x direction. (c) Calculated photonic band structure for a line defect with parameters a_1 and W1.

constant in the x direction was increased by 5 nm every two periods upon approaching the center (the lattice constant in the y direction was not changed). As a result, optical confinement regions are generated at the lower-frequency edge of the even-propagation band due to changes in the mode gap with x, as shown in Fig. 1(b).[20] Confinement for the odd-propagation band is achieved in a similar manner since crosstalk with the even-propagation mode is generally negligible. Accordingly, odd and even nanocavity modes are formed (several nanocavity modes can be formed for each propagation mode depending on the photonic parameters of the heterostructure).[26] A large number of higher-frequency resonant modes are also formed in both propagation bands by confinement of the PBG at the cavity edges. We refer to these as odd and even Fabry–Pérot (FP) modes because the line defect with 39 missing air holes can essentially be regarded as a FP cavity.[26–29] It should be emphasized that, in general, only the resonant modes associated with the even-propagation mode have been examined in studies on Raman Si lasers.[30,31] Here we additionally focus on the resonant modes that arise from the odd-propagation mode.

III. EXPERIMENTAL METHOD

Figure 2 shows the setup used for spectroscopic measurements. The light from a tunable cw laser was split into two beams. One beam was sent to a high-resolution wavelength meter. The other was modulated by a mechanical chopper at a frequency of ∼1 kHz with a 50% duty ratio and was focused by a 0.42-numerical-aperture (NA) objective lens on the facet of the excitation waveguide. The transmitted light from the opposite facet and the dropped light from the cavity in the direction vertical to the slab were collected by 0.40-NA lenses. The sample was placed on a high-precision 5-axis stage and the positions of the optical components were adjusted using near-infrared (NIR) cameras such that only the dropped and transmitted light passed through pinhole apertures, analogous to the situation in confocal microscopy. The intensities of the dropped and transmitted light were measured by lock-in amplifier systems as a function of the laser wavelength. Because the PBG for 2D-PCs is inactive for transverse magnetic (TM) polarization, incident and transmitted light with transverse electric (TE) polarization were used.

All resonant modes were excited by utilizing the even-propagation mode of the excitation waveguide because incident light on the waveguide facet easily couples to this mode (coupling to the odd-propagation mode is more difficult). We constructed several samples with different values of w and l in order to control the frequency of the even-propagation band and the magnitude of the evanescent mode coupling between the propagation mode and the resonant modes: one pair of samples had $w = 1.07$ W1 (W1 = 710 nm) and $l = 5$, 6, which were used for measuring the resonant modes near

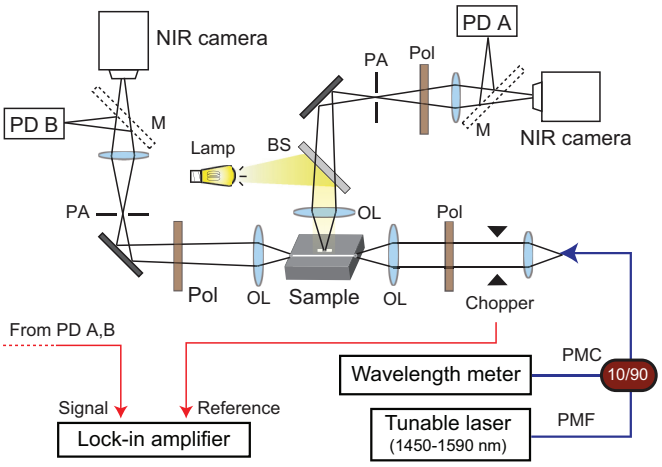

FIG. 2. (Color online) Setup for spectroscopic measurements. PMF, polarization maintaining fiber; PMC, polarization maintaining coupler; Pol, polarizer; OL, objective lens; BS, beam splitter; M, mirror on a flip-mount stage; PA, pinhole aperture; PD, InGaAs photodiode; NIR camera, near-infrared InGaAs camera.

the lower edge of the even-propagation band. A second pair of samples with $w = 0.95$ W1 and $l = 4, 5$ covered the middle frequency region. A third pair with $w = 0.91$ W1 and $l = 3, 4$ were used to investigate the higher-frequency region, including the odd-propagation band. All samples had the same cavity structure and were fabricated on the same chip.

IV. EXPERIMENTAL RESULTS

Figure 3(a) presents the frequencies (f) and Q values of all the resonant modes that were experimentally observed between 1450 nm ($f = 0.282$) and 1590 nm ($f = 0.258$). This range almost covers the odd- and even-propagation bands denoted in Fig. 1(c) where high-Q modes are formed (the Q factors are much lower above the light line). In Fig. 3(b) the dropped and transmitted spectra for the lowest-frequency mode at $f = 0.259$ are shown. Similar spectra were obtained for the other resonant modes. The Q values in Fig. 3(a) do not include the load of the excitation waveguide and were estimated from the wavelength (λ_0), linewidth ($\Delta\lambda$), and transmittance (T_0) at the resonant peak using the following relation:[32]

$$Q = \lambda_0/[\Delta\lambda\sqrt{T_0}]. \quad (1)$$

The open (blue) and solid (red) circles in Fig. 3(a) indicate resonant modes originating from the odd- and even-propagation modes, respectively. We were able to determine the origin of each mode using the polarization properties of the dropped light. Dropped light originating from the odd-propagation mode was polarized in the x direction whereas that from the even-propagation mode was polarized in the y direction, as shown in the insets. These properties can be explained by the far-field cancellation effect in E_x (E_y) for the even- (odd-) propagation mode.[27] The nanocavity modes were distinguished from the FP modes using their emission images. Emission from the nanocavity modes is located at the center of the heterostructure, whereas emission from the FP modes occurs at the cavity edges, as shown in Figs. 3(c) and 3(d). The lowest-frequency resonant modes in both the odd and even sets are the heterostructure nanocavity modes (solid lines). The higher-frequency modes are all FP modes (dashed lines). In summary, four types of resonant modes were observed, as expected: an even nanocavity mode, even FP modes, an odd nanocavity mode, and odd FP modes. The FP modes follow the FP resonance condition of $k_x = (\pi/L)\mathbf{m}$ for each propagation mode, where k_x is the wave vector, L is the cavity length, and $\mathbf{m}$ is the modal integer number. The dispersion curves presented in Fig. 1(c) determine the relation between k_x and f. Therefore, for most of the range, the modal number of the FP modes increases with frequency.[26–29] We note that fewer odd FP modes were observed than even FP modes because several of the odd FP modes were not spectrally resolved due to their small Q.

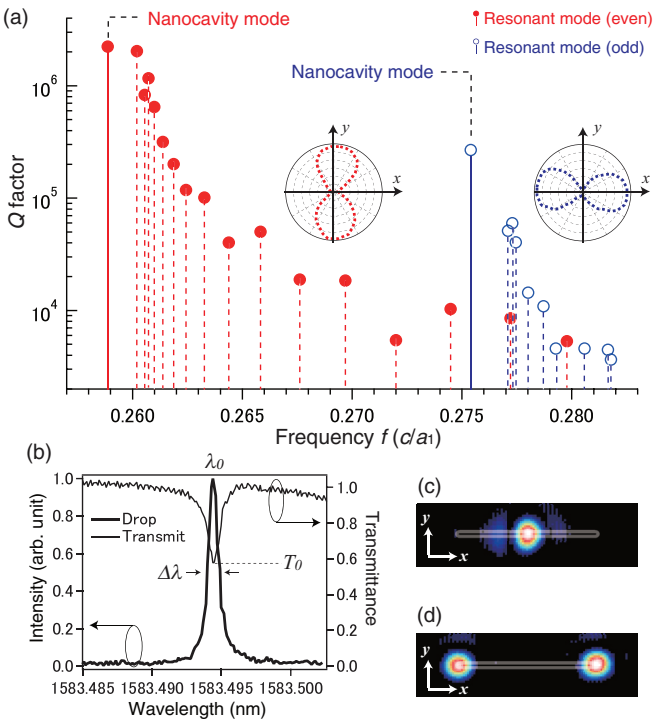

FIG. 3. (Color online) (a) Frequencies and Q values of all high-Q resonant modes in the heterostructure cavity. The insets show the polarization properties of the odd and even nanocavity modes. (b) Dropped and transmitted spectra for the even nanocavity mode. (c),(d) Near-field images for the odd nanocavity mode and the FP mode at $f = 0.2745$. Rectangles indicate the line defect forming the cavity.

V. DISCUSSION

We will now evaluate the applicability of the observed resonant modes to Raman Si lasers from the viewpoint of Q and f. A Raman Si laser requires two high-Q resonant modes to confine the pump light and the Stokes Raman-scattered light. We refer to these as the pump mode and Stokes mode, respectively, and we define the Q and f for the pump (Stokes) mode as Q_p and f_p (Q_S and f_S). To achieve lasing, the frequency spacing between the modes should be matched to the Si Raman shift of 15.6 THz. High Q factors are also important; Q_S is particularly significant in order to overcome the free carrier absorption loss associated with two-photon absorption (TPA). Because the Raman gain depends linearly on the pump power whereas the TPA-induced loss has a superlinear dependence, the Raman gain can be made to exceed the losses in the low pump region by increasing Q_S. Although the value of Q_S depends on a number of parameters (for example the free carrier lifetime, Raman gain coefficient, TPA coefficient, and modal overlap), we have experimentally confirmed that a Q_S of ~1 000 000 is required for cw operation (details will be reported elsewhere). Although such a high value is not required for Q_p, values larger than a few tens of thousands are advantageous for practical operation with a threshold less than several tens of μW.

In the lower-frequency range of Fig. 3(a), Q values of more than 1 000 000 were obtained for the even nanocavity mode and several of the even FP modes, which might also be candidates for the Stokes mode. In the higher-frequency range from which the pump mode should be selected, the odd nanocavity mode, odd FP modes, and even FP modes were all observed. We note that a separation of 15.6 THz from $f_S \cong 0.260$ is impossible

TABLE I. Resonant modes usable for the Stokes mode and pump mode for Raman Si lasers.

For Stokes mode	Q_S	For pump mode	Q_p
Even nanocavity mode $f = 0.259$	Highest $\gg 10^6$	Odd nanocavity mode $f = 0.275$	High $\gg 10^5$
Even FP mode $f = 0.260 \sim 0.261$	High $\geqslant 10^6$	Odd FP mode $f = 0.277 \sim 0.278$	Medium $10^4 \sim 10^5$

for pump modes with $f < 0.275$, even if a_1 is decreased to its lower limit for the operation wavelength of $\sim$1.2 μm which is determined by the band gap of Si. Because the Q factors of the even FP modes with $f > 0.275$ are less than 10 000, the odd nanocavity mode and odd FP modes at $f \cong 0.277$ emerge as candidates for the pump mode. Table I summarizes the possible Stokes and pump modes and indicates that the resonant mode originating from the even-propagation mode should be paired with that arising from the odd-propagation mode. The frequency spacing between these modes can be tuned to 15.6 THz by varying the air hole radius.[17]

Next, we consider the applicability of all four types of modes for SRS by examining the modal overlap of their electric fields. Figures 4(a)–4(f) show the calculated E_y for a line-defect cavity consisting of 39 missing air holes with a two-step heterostructure. The photonic parameters used in this FDTD calculation are the same as in Fig. 1. Figures 4(a)–4(c) show E_y for the first, second, and third resonant modes created by the even-propagation mode. The

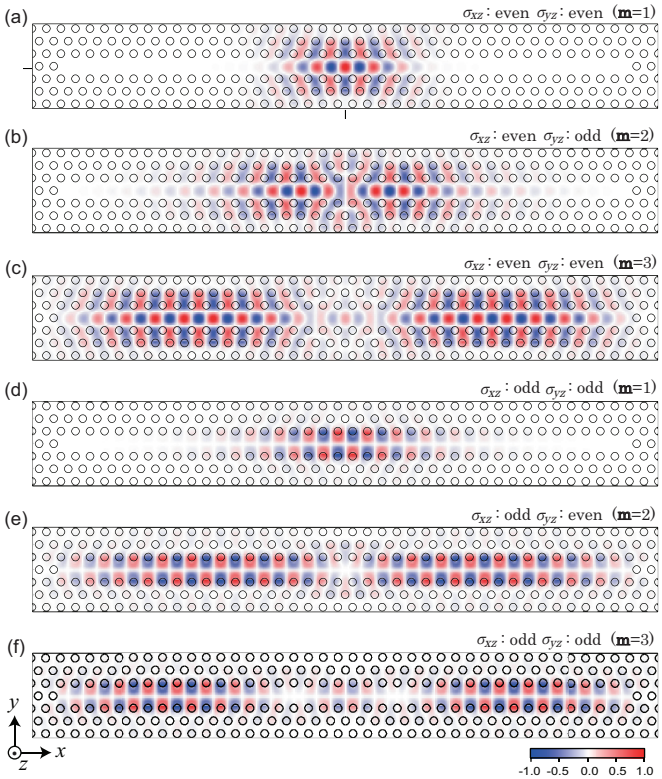

FIG. 4. (Color online) Calculated electric field distributions E_y for a heterostructure cavity consisting of 39 missing air holes. (a)–(c) Resonant modes generated by the even-propagation mode. (d)–(f) Resonant modes originating from the odd-propagation mode. The color scale represents the intensity of the electric field and **m** is the modal number. Symbols of σ_{xz} and σ_{yz} denote mirror planes.

modal numbers **m** for these modes are defined as **m** = 1, 2, and 3. Figures 4(d)–4(f) show E_y for the resonant modes arising from the odd-propagation mode. The distributions in Figs. 4(a) and 4(d) imply that the ground-state modes with **m** = 1 are the heterostructure nanocavity modes, in agreement with the experimental results.

A pair of pump and Stokes modes should have large modal overlap for efficient SRS. Here the modal symmetries of E_x and E_y, modal number **m**, Raman tensor of Si, and crystallographic direction in which the cavity is formed are important factors. As shown in Fig. 4, even-odd mode pairs with the same **m** have similar distributions in the x direction whereas mode pairs with different **m** have different distributions. Therefore, the former situation is favorable for large overlap. However, even-odd mode pairs have the opposite symmetries in E_y with respect to the xz plane (σ_{xz}) and yz plane (σ_{yz}) at the center of the defect. Although not shown here, this is also the case in E_x. These properties are favorable if we would fabricate the nanocavity along the [100] crystal direction on a (001) SOI substrate. This is because the SRS gain via the Raman tensor of Si is proportional to the following integral in such a cavity:[17]

$$\int_{\mathrm{Si}} |E^*_{x\_S} E_{y\_p} + E^*_{y\_S} E_{x\_p}|^2 dx dy dz. \tag{2}$$

Here the subscripts S and p indicate the Stokes and pump modes, and the label Si refers to the integral excluding the air holes. The overlap integrals between the cross components are important in Eq. (2) and the cross components for even-odd mode pairs with the same **m** have the same symmetry. In contrast, the SRS gain is proportional to the overlap integrals between the same components for a cavity fabricated along the [110] direction:

$$\int_{\mathrm{Si}} |E^*_{x\_S} E_{x\_p} - E^*_{y\_S} E_{y\_p}|^2 dx dy dz. \tag{3}$$

In this situation the combination of even-odd mode pairs in unfavorable. In addition, the negative terms are disadvantageous for any pair of modes. The relative magnitudes of the Q factors displayed in Table I are insensitive to the direction of fabrication ([100] or [110]) because both the periodic refractive

TABLE II. Magnitudes of Eq. (2) for even-odd resonant mode pairs with **m** = 1 to 3. These values are normalized by the value for a pair of ground-state nanocavity modes.

Resonant mode	Odd **m** = 1	Odd **m** = 2	Odd **m** = 3
Even **m** = 1	1	0.07	0.06
Even **m** = 2	0.47	0.20	0.05
Even **m** = 3	0.05	0.28	0.30

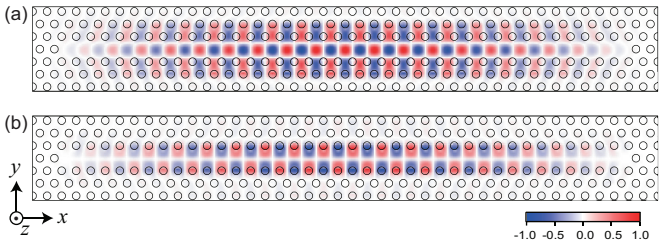

FIG. 5. (Color online) Calculated E_y of the ground-state FP modes generated by (a) the even-propagation mode and (b) the odd-propagation mode for a FP cavity consisting of 39 missing air holes without any heterostructure.

index variation (which determines the properties of the PC) and the accuracy of fabrication are insensitive to the direction.

Table II presents the relative magnitudes of Eq. (2) for the pairs of even-odd resonant modes shown in Figs. 4(a)–4(f). Here we neglect the integral in the z direction. The pair of ground-state nanocavity modes [Figs. 4(a) and 4(d)] has the largest value due to their high degree of overlap and small modal volume. The other even-odd mode pairs with the same $\mathbf{m}$ have moderately large values despite their larger modal volume, while most of the even-odd mode pairs with different $\mathbf{m}$ have small values. Because the even $\mathbf{m} = 2$ resonant mode is also confined by the heterostructure, combination with the odd $\mathbf{m} = 1$ mode also yields a relatively large value. The pair comprising the even $\mathbf{m} = 3$ and odd $\mathbf{m} = 2$ modes also has moderately large value because the electric field of the even $\mathbf{m} = 3$ mode is strongly distributed near the edges of the line defect due to the heterostructure. We note that the magnitude of the integral in Eq. (2) can be increased for pairs other than the two ground-state nanocavity modes by decreasing the length of the FP cavity; however, the Q values then rapidly decrease.[28] Both the degree of overlap and the Q values of the ground-state nanocavity modes are relatively insensitive to the length of the FP cavity. The magnitudes of the integral in Eq. (3) for even-odd mode pairs are 10 to 20 times smaller than Eq. (2).

In our previous demonstration of a Raman Si laser, we utilized the pair of ground-state nanocavity modes. Our discussion above suggests that some of the other even-odd mode pairs also have potential for cw lasing due to their significant degree of overlap and the high experimental Q values in Fig. 3(a). However, controlling the frequencies of the FP modes would be more difficult than for the nanocavity modes due to the long cavity length and the influence of partial mirrors at the heterostructure interfaces. Furthermore, the free spectral range (FSR) for the lower-order FP modes is smaller than that of the nanocavity modes in Fig. 3(a).

We can conclude that using the ground-state nanocavity modes originating from the odd- and even-propagation modes is the best choice. The highest-reported experimental Q value for the even nanocavity mode is ~4 000 000 and precise control of the resonant wavelength has been demonstrated.[24] The odd ground-state nanocavity mode has the highest Q in the series of resonant modes associated with the odd-propagation mode. A relatively large FSR is advantageous for experimental investigations and for stable single-mode operation.

Finally, it is interesting to note the potential of FP modes that arise in a line-defect cavity without any heterostructure. Figure 5 shows the E_y of the ground state FP modes ($\mathbf{m} = 1$) originating from the even- and odd-propagation modes in such a cavity. The magnitude of the integral in Eq. (2) for this pair is 30% smaller than that for the pair shown in Figs. 4(a) and 4(d) due to the larger modal volume. However, the calculated Q factors are as high as 2×10^7 and 6×10^5, respectively. By applying techniques to increase the Q factors by shifting the air hole positions,[19,33] sufficiently high Q values for lasing will be obtained even in FP cavities with shorter lengths. Raman lasing with high output power will be expected for this design due to the large volume.

VI. SUMMARY

We have studied the optical properties of high-Q resonant modes in a PC heterostructure cavity in order to investigate their applicability to Raman Si lasers. Four types of resonant modes were observed, which have highest Q factors near the lower edges of the original propagation bands. After consideration of all the relevant factors, the pair of ground-state heterostructure nanocavity modes that originate from the first-order (even) and second-order (odd) propagation modes is the most suitable combination for Raman Si lasers. A pair of higher-order modes might also have some potential. The optical properties reported in this paper will be helpful in studies of Raman Si lasers or amplifiers in other types of PC devices.[22,29,34–40]

ACKNOWLEDGMENTS

Y.T. is supported by NanoSquare program, Funds for the Development of Human Resources in Science and Technology commissioned by MEXT. This work was supported by JST, PRESTO, by MEXT KAKENHI (Grants No. 23104721 and No. 21104512), JSPS KAKENHI (Grant No. 23686015 and No. 20226002), Future Pioneering Projects, and the CPHoST program.

*y-takahashi@21c.osakafu-u.ac.jp
†These authors contributed equally to this work.
‡snoda@kuee.kyoto-u.ac.jp

[1] S. S. Iyer and Y.-H. Xie, Science **260**, 40 (1993).
[2] R. Claps, D. Dimitropoulos, Y. Han, and B. Jalali, Opt. Express **10**, 1305 (2002).
[3] B. Jalali and S. Fathpour, J. Lightwave Technol. **24**, 4600 (2006).
[4] J. Leuthold, C. Koos, and W. Freude, Nat. Photonics **4**, 535 (2010).
[5] R. Claps, D. Dimitropoulos, V. Raghunathan, Y. Han, and B. Jalali, Opt. Express **11**, 1731 (2003).
[6] R. Espinola, J. Dadap, R. Osgood, S. McNab, and Y. Vlasov, Opt. Express **12**, 3713 (2004).

[7]A. Liu, H. Rong, M. Paniccia, O. Cohen, and D. Hak, Opt. Express **12**, 4261 (2004).
[8]Q. Xu, V. Almeida, and M. Lipson, Opt. Express **12**, 4437 (2004).
[9]O. Boyraz and B. Jalali, Opt. Express **12**, 5269 (2004).
[10]M. Krause, H. Renner, and E. Brinkmeyer, Opt. Express **12**, 5703 (2004).
[11]T. Liang and H. Tsang, Appl. Phys. Lett. **85**, 3343 (2004).
[12]R. Jones, H. Rong, A. Liu, A. Fang, M. Paniccia, D. Hak, and O. Cohen, Opt. Express **13**, 519 (2005).
[13]H. Rong, A. Liu, R. Jones, O. Cohen, D. Hak, R. Nicolaescu, A. Fang, and M. Paniccia, Nature (London) **433**, 292 (2005).
[14]H. Rong, R. Jones, A. Liu, O. Cohen, D. Hak, A. Fang, and M. Paniccia, Nature (London) **433**, 725 (2005).
[15]T. Liang and H. Tsang, Appl. Phys. Lett. **84**, 2745 (2004).
[16]H. Rong, S. Xu, Y. Kuo, V. Sih, O. Cohen, O. Raday, and M. Paniccia, Nat. Photonics **1**, 232 (2007).
[17]Y. Takahashi, Y. Inui, M. Chihara, T. Asano, R. Terawaki, and S. Noda, Nature (London) **498**, 470 (2013).
[18]S. Noda, A. Chutinan, and M. Imada, Nature (London) **407**, 608 (2000).
[19]Y. Akahane, T. Asano, B. S. Song, and S. Noda, Nature (London) **425**, 944 (2003).
[20]B. S. Song, S. Noda, T. Asano, and Y. Akahane, Nat. Mater. **4**, 207 (2005).
[21]D. Englund, I. Fushman, and J. Vuckovic, Opt. Express **13**, 5961 (2005).
[22]E. Kuramochi, M. Notomi, S. Mitsugi, A. Shinya, T. Tanabe, and T. Watanabe, Appl. Phys. Lett. **88**, 041112 (2006).
[23]Y. Takahashi, Y. Tanaka, H. Hagino, T. Sugiya, Y. Sato, T. Asano, and S. Noda, Opt. Express **17**, 18093 (2009).
[24]Y. Taguchi, Y. Takahashi, Y. Sato, T. Asano, and S. Noda, Opt. Express **19**, 11916 (2011).
[25]R. Terawaki, Y. Takahashi, M. Chihara, Y. Inui, and S. Noda, Opt. Express **20**, 22743 (2012).
[26]Y. Takahashi, Y. Tanaka, H. Hagino, T. Asano, and S. Noda, Appl. Phys. Lett. **92**, 241910 (2008).
[27]S. H. Kim, G. H. Kim, S. K. Kim, H. G. Park, and Y. H. Lee, J. Appl. Phys. **95**, 411 (2004).
[28]M. Okano, T. Yamada, J. Sugisaka, N. Yamamoto, M. Itoh, T. Sugaya, K. Komori, and M. Mori, J. Opt. (Bristol, UK) **12**, 075101 (2010).
[29]M. Felici, K. A. Atlasov, A. Surrente, and E. Kapon, Phys. Rev. B **82**, 115118 (2010).
[30]X. Yang and C. Wong, Opt. Express **13**, 4723 (2005); **15**, 4763 (2007).
[31]H. Takano, T. Asano, and S. Noda, *Spring Meeting Japan Society of Applied Physics*, Abstract 29a-ZB-8 (The Japan Society of Applied Physics, Bunkyo-ku, Tokyo, Japan, 2007).
[32]A. Chutinan, M. Mochizuki, M. Imada, and S. Noda, Appl. Phys. Lett. **79**, 2690 (2001).
[33]T. Nakamura, T. Asano, and S. Noda, *Spring meeting Japan Society of Applied Physics*, Abstract 26p-KA-8 (The Japan Society of Applied Physics, Bunkyo-ku, Tokyo, Japan, 2011).
[34]J. McMillan, M. Yu, D. Kwong, and C. Wong, Appl. Phys. Lett. **93**, 251105 (2008).
[35]M. Notomi, E. Kuramochi, and H. Taniyama, Opt. Express **16**, 11095 (2008).
[36]P. B. Deotare, M. W. McCutcheon, I. W. Frank, M. Khan, and M. Loncar, Appl. Phys. Lett. **94**, 121106 (2009).
[37]X. Checoury, M. Kurdi, Z. Han, and P. Boucaud, Opt. Express **17**, 3500 (2009).
[38]X. Checoury, Z. Han, and P. Boucaud, Phys. Rev. B **82**, 041308 (2010).
[39]I. H. Rey, Y. Lefevre, S. A. Schulz, N. Vermeulen, and T. F. Krauss, Phys. Rev. B **84**, 035306 (2011).
[40]H. Sumikura, E. Kuramochi, H. Taniyama, and Masaya Notomi, Appl. Phys. Lett. **102**, 231110 (2013).